ADVANCED MATERIALS
www.advmat.de

Dodecaborane-Based Dopants Designed to Shield Anion Electrostatics Lead to Increased Carrier Mobility in a Doped Conjugated Polymer

Taylor J. Aubry, Jonathan C. Axtell, Victoria M. Basile, K. J. Winchell, Jeffrey R. Lindemuth, Tyler M. Porter, Ji-Yuan Liu, Anastassia N. Alexandrova, Clifford P. Kubiak, Sarah H. Tolbert, Alexander M. Spokoyny,* and Benjamin J. Schwartz**

One of the most effective ways to tune the electronic properties of conjugated polymers is to dope them with small-molecule oxidizing agents, creating holes on the polymer and molecular anions. Undesirably, strong electrostatic attraction from the anions of most dopants localizes the holes created on the polymer, reducing their mobility. Here, a new strategy utilizing a substituted boron cluster as a molecular dopant for conjugated polymers is employed. By designing the cluster to have a high redox potential and steric protection of the core-localized electron density, highly delocalized polarons with mobilities equivalent to films doped with no anions present are obtained. AC Hall effect measurements show that P3HT films doped with these boron clusters have conductivities and polaron mobilities roughly an order of magnitude higher than films doped with F_4TCNQ, even though the boron-cluster-doped films have poor crystallinity. Moreover, the number of free carriers approximately matches the number of boron clusters, yielding a doping efficiency of ≈100%. These results suggest that shielding the polaron from the anion is a critically important aspect for producing high carrier mobility, and that the high polymer crystallinity required with dopants such as F_4TCNQ is primarily to keep the counterions far from the polymer backbone.

Creating electrical carriers by doping in a controlled fashion enables semiconductors to be used in a wide variety of optoelectronic applications. Indeed, doped conjugated polymers are found in commercially available organic light-emitting diode (OLED) displays,[1] used to enhance organic solar cells[2] and field-effect transistors,[3] and are receiving increased attention for thermoelectric applications.[4–9] Doping of conjugated polymers can be achieved by electrochemical[10] or electrical charge injection[11] methods, but chemical doping is the best method to produce stable carriers without the need for a continuously applied potential. Chemical doping involves the introduction of a strong electron acceptor (oxidizing agent, for p-type doping) or a strong electron donor (reducing agent, for n-type doping) that can undergo a charge transfer reaction with the polymer,[12] creating charge carriers on the polymer chain while the dopant molecules remain in the film as

T. J. Aubry, Dr. J. C. Axtell, V. M. Basile, K. J. Winchell, J.-Y. Liu, Prof. A. N. Alexandrova, Prof. S. H. Tolbert, Prof. A. M. Spokoyny, Prof. B. J. Schwartz
Department of Chemistry and Biochemistry
University of California, Los Angeles
Los Angeles, CA 90095-1569, USA
E-mail: tolbert@chem.ucla.edu; spokoyny@chem.ucla.edu; schwartz@chem.ucla.edu

Dr. J. R. Lindemuth
Lake Shore Cryotronics
Westerville, OH 43082, USA

T. M. Porter, Prof. C. P. Kubiak
Department of Chemistry and Biochemistry
University of California, San Diego
La Jolla, CA 92093, USA

The ORCID identification number(s) for the author(s) of this article can be found under https://doi.org/10.1002/adma.201805647.

DOI: 10.1002/adma.201805647

J.-Y. Liu
Key Laboratory for Advanced Materials
Center for Computational Chemistry and Research Institute of Industrial Catalysis
School of Chemistry and Molecular Engineering
East China University of Science and Technology
Shanghai 200237, P. R. China

Prof. A. N. Alexandrova, Prof. S. H. Tolbert, Prof. A. M. Spokoyny, Prof. B. J. Schwartz
California NanoSystems Institute
University of California, Los Angeles
Los Angeles, CA 90095-1569, USA

Prof. S. H. Tolbert
Department of Materials Science and Engineering
University of California, Los Angeles
Los Angeles, CA 90095-1569, USA

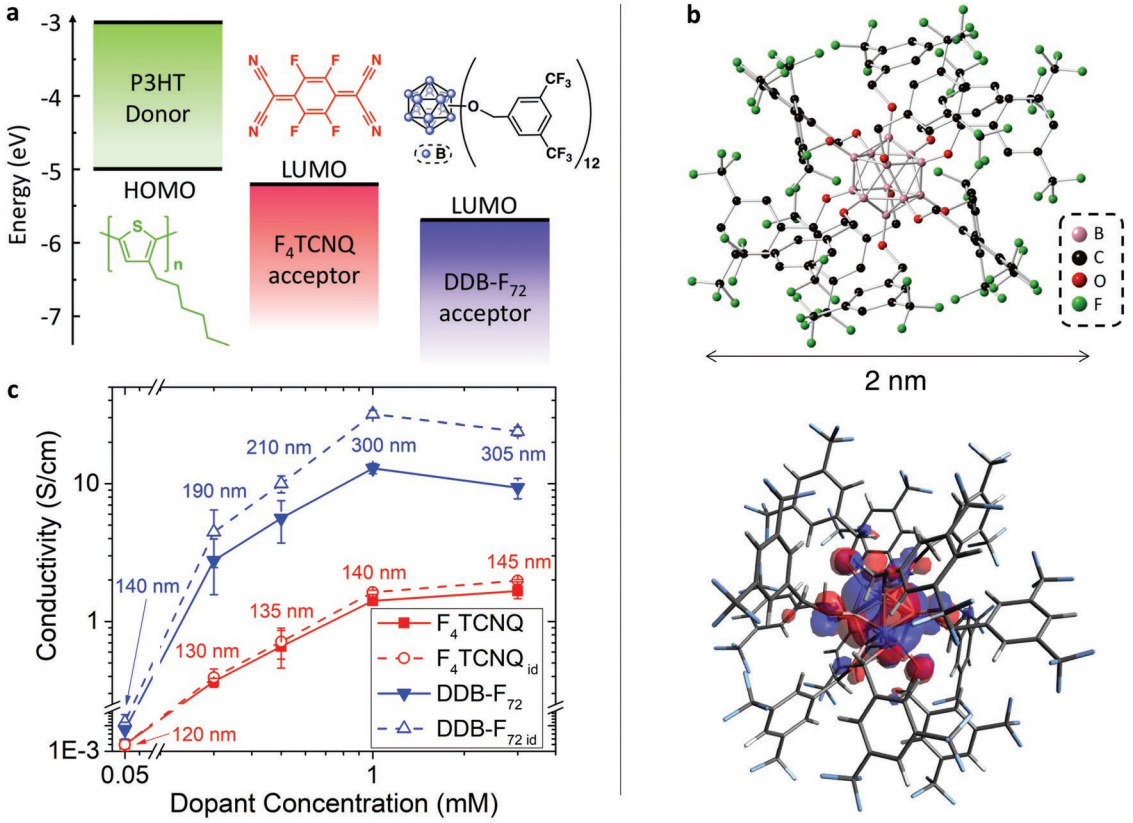

Figure 1. a) Chemical structures and schematic energy diagram of P3HT, F_4TCNQ, and DDB-F_{72} showing ≈0.5 V greater offset for DDB-F_{72} than F_4TCNQ. b) (Top) Ball-and-stick representation of the X-ray crystal structure of DDB-F_{72}; (bottom) DDB-F_{72} anion SOMO calculated by TD-DFT showing the electron localized on the DDB core. c) Conductivities (solid symbols, calculated using the measured thickness) and idealized conductivities (open symbols, calculated using the 120 nm original thickness) of P3HT films doped with F_4TCNQ (red symbols) and DDB-F_{72} (blue symbols) via solution sequential doping. The error bars are the standard deviation calculated from at least three samples. At the same dopant concentration, DDB-F_{72} produces conductivities that are an order of magnitude higher than those produced by F_4TCNQ.

counterions. Most conjugated polymers are p-type semiconductors, with positive carriers (holes, often referred to as polarons) created by oxidizing dopants.

Some of the earliest molecular dopants for conjugated polymers were halogen vapors,[12] but the instability of the doped films produced this way has led to the design of more stable molecular dopants.[13] One of the most popular molecular dopants for conjugated polymers is 2,3,5,6-tetrafluoro-7,7,8,8-tetracyanoquinodimethane (F_4TCNQ);[4–9,14–22] see **Figure 1**a (red) for chemical structure. F_4TCNQ has a low-lying lowest unoccupied molecular orbital (LUMO), (–5.2 eV vs vacuum)[23] giving it the ability to p-dope a wide variety of conjugated polymers, including poly(3-hexylthiophene-2,5-diyl) (P3HT), whose chemical structure is shown in Figure 1a (green). Unlike doped inorganic semiconductors, where the interactions of substitutional impurities with the generated charge carriers are screened, the majority of the doping-induced carriers in conjugated polymers remain Coulomb-bound to the dopant counterions due to the low permittivity of organic materials.[16–18] For P3HT doped with F_4TCNQ, it has been estimated that even though the majority of F_4TCNQ molecules undergo integer charge transfer with P3HT, 95% of the holes that are created remain bound to their counterions[16] and thus do not contribute to electrical conduction. Indeed, strong electrostatic interactions between polarons and their counterions are known to localize polarons and reduce their mobilities.[15]

To overcome this issue of carrier localization, in this work we describe a perfunctionalized dodecaborane cluster that was designed to spatially separate the anions created when doping conjugated polymers. Dodecaborane (DDB) clusters are robust and kinetically stable due to their 3D aromaticity, which allows for electron delocalization around the boron scaffold.[24–28] Certain perfunctionalized clusters of the type $B_{12}(OR)_{12}$ (R = alkyl, aryl, H) behave as reversible, redox-active species with multiple accessible oxidation states.[27–31] Recent advances have led to the rational and rapid synthesis of such substituted dodecaboranes with tunable redox potentials.[29] We have designed a DDB cluster with a very high ground-state redox potential, which when combined with the cluster's intrinsic stabilization of electron density in its well-shielded core, makes it an outstanding candidate to molecularly dope conjugated polymers.

The conventional processing method to dope polymeric semiconductors, known as blend doping, involves mixing the polymer and dopant in solution prior to casting the doped polymer onto a substrate. The solvents for most conjugated polymers, however, are nonpolar, such that at high doping levels the charges produced on the polymer and dopant render them insoluble during solution processing, yielding very

poor doped film quality. This problem has been overcome by sequential doping,[5–9,14,15,19–22,32,33] which relies on exposing a precast polymer film to the dopant, either in the vapor phase[5–8,20,22,32,33] or in solution.[14] Solution sequential processing uses a semiorthogonal solvent to swell but not dissolve the polymer underlayer, allowing mass action to drive the dopant into the swollen polymer film.[5,6,8,9,14,15,19–21] Doping by solution sequential processing (SqP) maintains all of the advantages of solution-based processing methods, producing high-quality films with conductivities that are significantly better than those produced by blend doping.[14,19] We expect that SqP should be amenable for use with dodecaborane clusters given that it is routinely used to infiltrate large molecules such as fullerenes and large dopants into films of conjugated polymers.[34–38]

Here, we report the use of a newly synthesized, strongly oxidizing perfunctionalized DDB cluster as a dopant for the conjugated polymer P3HT. The chemical structure of our new cluster, shown in Figure 1a (blue), depicts the pseudo-icosahedral dodecaborane core with each vertex functionalized with a 3,5-bis(trifluoromethyl)benzyloxy substituent. We refer to this molecule as DDB-F_{72} because of the 72 electron-withdrawing F atoms placed on the periphery of the cluster. Using SqP to dope identical films of P3HT with both DDB-F_{72} and F_4TCNQ, we find that at equimolar doping concentrations, DDB-F_{72} produces doped films with conductivities that are an order of magnitude higher. We verify using NMR spectroscopy techniques that there is negligible electron transfer between DDB-F_{72} clusters, so that the conductivity improvement we see comes solely from the increased mobility of polarons on the conjugated polymer.

To understand this increased conductivity, we structurally characterize our doped polymer films by using X-ray photoelectron spectroscopy (XPS) and 2D grazing-incidence wide-angle X-ray scattering (2D-GIWAXS) to show that DDB-F_{72}-doped P3HT films are remarkably noncrystalline, likely due to the fact that the DDB cluster cannot intercalate into the crystalline polymer domains due to its large size. This is in sharp contrast to dopants such as F_4TCNQ, which reside within the polymer crystallites[9,15] in closer proximity to the polarons. In addition to residing farther from the polymer crystallites, the steric footprint associated with DDB-F_{72}'s peripheral substitutions, in combination with the delocalization of the unpaired electron within the shielded boron cluster core, allows for greatly reduced electrostatic interactions between DDB-F_{72} anions and the holes on the polymer chains.

With this reduced electrostatic interaction, we show using combination of AC Hall effect and IR spectroscopy measurements that the polarons on P3HT doped with DDB-F_{72} have mobilities that are an order of magnitude higher than those created by doping with F_4TCNQ; the carrier mobilities with DDB-F_{72} are comparable to those created by charge modulation with no anions present at all.[11] We calculate idealized conductivities in our DDB-F_{72}-doped P3HT films of 32 S cm^{-1}, despite the lack of crystallinity in our doped material. These findings highlight the importance of polaron delocalization effects and the corresponding need to electrostatically screen the anion from the holes. Reducing the polaron/counterion Coulomb interaction is clearly important for electrical conduction. We suspect the reason that high crystallinity is important for good conductivity with dopants such as in F_4TCNQ that it also reduces the Coulomb interaction. This is because when F_4TCNQ enters the polymer crystallites, it happens to sit in the lamellar regions among the polymer side chains so that the anion is held a fair distance away from the polymer backbone where the polaron resides, so that high crystallinity leads to a reduced Coulomb interaction. In contrast, our tailored DDB dopants are so large that they can only infiltrate amorphous regions, but electrostatic shielding is taken care of by the dopant itself so that polymer crystallinity is no longer required.

We chose P3HT for this study as it is a model conjugated polymer that has become an important reference material for the study of optoelectronic processes in organic semiconductors. The offset between the highest occupied molecular orbital (HOMO) of the polymer and LUMO of the dopant gives the energetic driving force for doping via integer charge transfer.[16] Figure 1a shows these energy levels for P3HT, F_4TCNQ, and DDB-F_{72} based on cyclic voltammetry (CV) measurements of the dopants (see Figure S6 in the Supporting Information) and literature values for P3HT.[39] Our CV measurements indicate a $0/1^-$ redox potential of 0.16 V versus F_c/F_c^+ for F_4TCNQ, in excellent agreement with literature values.[40] The redox potential of DDB-F_{72} is 0.67 V versus F_c/F_c^+, thus producing a 0.5 eV greater energetic driving force for doping compared to F_4TCNQ.

The X-ray crystal structure of DDB-F_{72} is shown in Figure 1b (top) (see the Supporting Information for CIF file). The diameter of DDB-F_{72} is ≈2 nm, nearly twice that of a C_{60} molecule. The B_{12}-based core lies deep in the center of the cluster, surrounded by the corona of 12 bulky substituents, so if the additional unpaired electron on the reduced cluster is confined to the core as expected,[29,31] we should be able to achieve increased spatial separation of the electron from the polaron. Indeed, our time-dependent density functional theory (TD-DFT) calculations reveal that the singly occupied molecular orbital (SOMO) of the DDB-F_{72} anion is delocalized only on the core, as shown in Figure 1b (bottom).

To dope conjugated polymer films via SqP, we started by spinning 120 nm thick P3HT films out of 1,2-dichorobenzene at 1000 rpm for 60 s. We then spun the dopant (F_4TCNQ or DDB-F_{72}) out of solutions with different concentrations in dichloromethane (DCM) at 4000 rpm for 10 s on top of the precast polymer film. We measured the electrical conductivity of the doped films using the Van der Pauw method,[41] a type of four-point-probe measurement, with the electrodes placed at the corners of a 1.5 cm × 1.5 cm square (see the Supporting Information for details). The results are shown in Figure 1c.

The filled points/solid curves in Figure 1c show that for the same molar concentration of dopant, the conductivities of P3HT films doped with DDB-F_{72} (blue down-pointing triangles) are about an order of magnitude higher than the F_4TCNQ-doped samples (red squares). For example, at 1×10^{-3} M dopant concentrations, we achieve P3HT conductivities of 12.9 S cm^{-1} when doped with DDB-F_{72} but only 1.4 S cm^{-1} when doped with F_4TCNQ. We were unable to explore SqP doping concentrations higher than a few millimolar because of the solubility limit of both dopants in DCM. The drop in conductivity observed for 3×10^{-3} M DDB-F_{72} solutions is due to their colloidal nature, which is above the molecular solubility limit; the colloidal solutions do not effectively deliver dopant in the

P3HT film, as documented in the spectroscopy section of the Supporting Information. The DDB-F_{72}-doped films are stable under inert atmosphere for days (see the Supporting Information), suggesting the films would remain stable indefinitely if packaged appropriately.

One interesting feature of SqP is that so much of the large DDB-F_{72} dopant can be intercalated that the polymer films change thickness after doping.[34] Starting with 120 nm thick pre-cast P3HT films, we find that doping with a 1×10^{-3} M solution yields 140 nm thick films doped with F_4TCNQ but 300 nm thick films doped with DDB-F_{72}. Since SqP relies on swelling of the polymer followed by infiltration of the dopant into the swollen polymer matrix,[35] we worried about whether or not DDB-F_{72} was fully penetrating into the P3HT film. Given the large size of the DDB-F_{72} molecule and the fact that some large dopants have shown limited film penetration in previous work,[42] it is possible that the large increase in thickness we observe results from an overlayer of excess DDB-F_{72} on top of the P3HT film rather than uniform intercalation throughout the film.

To investigate the penetration of the dopant into the film, we used XPS, which has a penetration depth of only a few nm, to examine the oxidation state of boron near the top surface of the film. **Figure 2** shows the B 1s XPS spectra of both the neutral DDB-F_{72} cluster (black curve) and the DDB-F_{72} anion (red curve), along with one of our DDB-F_{72}-doped P3HT films (blue curve). The data make clear that the boron on the top surface of our films is reduced, suggesting that there is no excess overlayer of neutral clusters on top of the film, and that the clusters have indeed penetrated well into the P3HT layer. Further evidence that there is no continuous cluster overlayer is that XPS is able to pick up considerable signal from the sulfur of P3HT on the top surface of this doped film (see Table S3 in the Supporting Information). In addition, we imaged the top surface of the films using both optical and scanning electron microscopies (SEM) (see Figures S9 and S10 of the Supporting Information). In the optical images, we see sparse crystallites of DDB-F_{72} that certainly do not form a contiguous overlayer. The SEM images reveal a sharp crack pattern, which we attribute as resulting from the expansion and contraction of the film upon swelling and deswelling during the SqP process.

To further our understanding of the degree of cluster penetration, we also examined the elemental composition of both the top and bottom surfaces of our DDB-F_{72}-doped P3HT films using XPS; we accessed the bottom surfaces by floating doped films off the substrate,[34] as described in more detail in the Supporting Information. Since sulfur is unique to P3HT while boron and fluorine are unique to DDB-F_{72}, the sulfur 2p:boron 1s and sulfur 2p:fluorine 1s peak-integrated ratios, shown in the inset to Figure 2a, give a good measure of the film composition at each surface. The data make clear that the B:S and F:S ratios on the top and bottom of the DDB-F_{72}-doped films are similar, suggesting that the clusters are roughly evenly distributed throughout the film. Indeed, recent work has shown that other fairly large dopant molecules also are able to penetrate well into pre-cast P3HT films.[37] Moreover, the XPS peak position for boron on both the top and bottom film surfaces indicate the cluster is reduced throughout the film (see the Supporting Information for detailed XPS peak fit assignments and additional information).

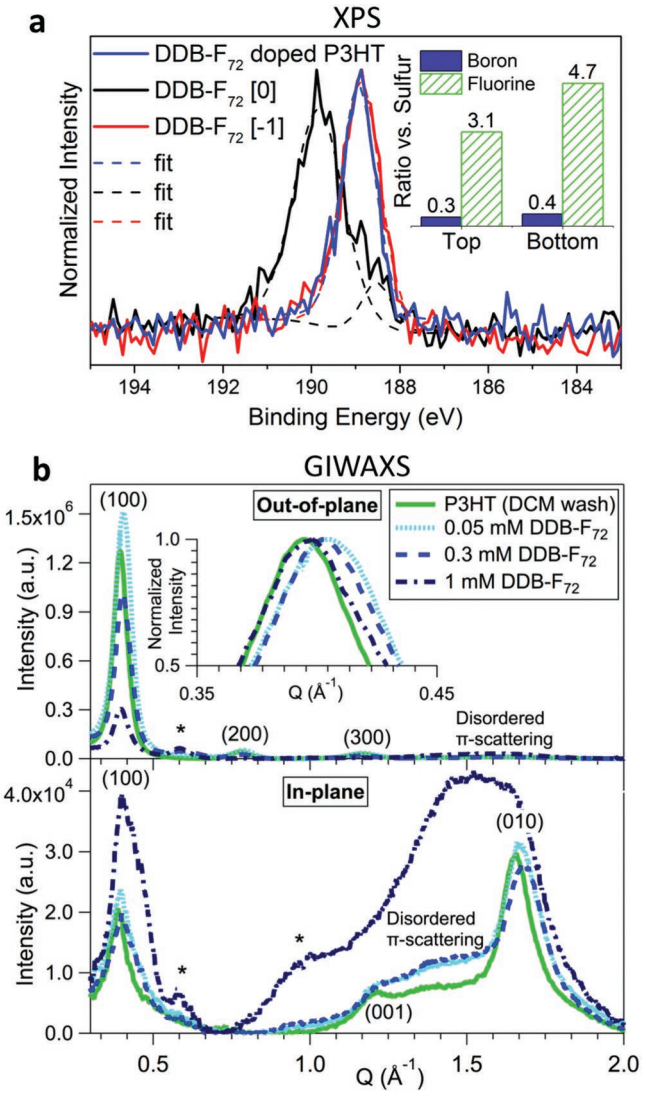

Figure 2. Structural characterization of DDB-cluster-doped films. a) B 1s XPS spectra of the top surface of pure DDB-F_{72} films in the neutral [0, black curve] and anionic [–1, red curve] states, overlaid with that of a DDB-F_{72}-doped P3HT film (blue curve). The overlap of the doped film and anion spectra indicates that the clusters at the top surface of the film are all reduced. (Inset) XPS-determined B:S and F:S ratios measured at the top and bottom of DDB-F_{72}-doped P3HT films indicating that the clusters penetrate the film. b) Out-of plane (top) and in-plane (bottom) 2D-GIWAXS spectra for films of pure P3HT (green curves) and DDB-F_{72}-doped P3HT (blue curves). (Inset) Zoomed in view of the (100) peak. Dopant-induced peaks are denoted by asterisks (*). These data indicate DDB-F_{72} does not enter the crystallites given its large size and at high dopant concentration (dark blue dashed-dotted curves), there is significant loss of overall crystallinity.

It is important to note that the calculation of electrical conductivity from the measured sheet resistivity scales inversely with the thickness of a material. Given the large thickness change of our DDB-F_{72}-doped films, this makes the conductivities we measure all the more remarkable because electrical conduction takes place only on the polymer, but the

polymer comprises only ≈1/3 of the material in the DDB-F_{72}-doped films. To verify the conduction mechanism, we investigated the kinetics of electron self-exchange between $[DDB\text{-}F_{72}]^0$ and $[DDB\text{-}F_{72}]^{-1}$ by dynamic NMR line broadening experiments, described in more detail in the Supporting Information. Using ^{19}F NMR across a range of 40 °C, we observed no coalescence of the peaks corresponding to the neutral and anionic forms of DDB-F_{72} in solution, indicating an electron self-exchange rate slower than that of the experimental timescale ($k_{ET} < 1.2 \times 10^3$ s^{-1} or $\tau_{ET} > 0.84$ ms), which is orders of magnitude longer than the typical collision time between clusters. This indicates that there is a high intrinsic barrier to electron transfer between DDB-F_{72} clusters, most likely the result of small electronic couplings due to poor orbital overlap between self-exchanging pairs.[43–45] Indeed, the idea of poor electron transfer between DDB clusters is in agreement with our TD-DFT calculations in Figure 1b, which show strong localization of the electron in the cluster interior, likely due to stabilization from the aromaticity of the B_{12} cluster. Overall, our NMR measurements strongly imply that electron hopping between DDB clusters does not occur on any reasonable timescale, and therefore the electrical conduction of our doped films takes place only through the polymer network.

Given that the doped films are 300 nm thick but that there is only an initially 120 nm thickness of polymer material in the doped film to conduct, we calculated "idealized conductivities" based on the initial polymer thickness of 120 nm rather than using the measured doped film thickness. These idealized conductivities, which represent the limit of conductivity that could be achieved with the same carrier mobility if there were no swelling of the film during doping, are shown by the dotted lines and open symbols in Figure 1c. The difference between the idealized conductivity and the conductivity is larger for the DDB-F_{72}-doped films due to their larger thickness increase. At the 1×10^{-3} M dopant concentration, we achieve idealized conductivities of ≈32 S cm^{-1} for the DDB-F_{72}-doped films, whereas the idealized conductivity of F_4TCNQ-doped films reaches only 2.0 S cm^{-1}.

To better understand the structure of our DDB-F_{72}-doped films, we used 2D GIWAXS. Figure 2b shows the out-of-plane (top) and in-plane (bottom) scattering patterns of P3HT (green solid curves) and P3HT doped with DDB-F_{72} from low-to-high concentration (light-to-dark blue curves). As expected for pure P3HT, which is well known to have a preferential edge-on orientation,[8,19,20] we see that the intensity of the π–π stacking (010) peak is largely in-plane, while strong peak intensity is observed in the out-of-plane direction for the lamellar (h00) peaks, indicating edge-on orientation with respect to the substrate.

Upon doping with DDB-F_{72} with low-to-mid concentration solutions (0.05 and 0.3×10^{-3} M), we see that the edge-on orientation of P3HT's crystallites is maintained as the (010) peak is still largely in-plane, consistent with the fact that SqP is known to preserve domain orientation.[14,15,36] The in-plane data reveals a shift in the (010) peak to higher Q, reminiscent of what has been previously reported for F_4TCNQ,[9,15] but with some significant differences.

In F_4TCNQ-doped-P3HT, a much larger shift of the (010) π-stacking peak, out to 1.8 Q, is observed upon doping compared to what is seen here. Despite the large peak shift, the change in the π-stacking distance is actually quite small as the structural change is mainly due to reorientation of the unit cell: F_4TCNQ intercalation into the side-chain regions of the P3HT crystallites causes an adjustment of the chain angle relative to the unit cell axes.[9] DDB-F_{72} only causes a small shift of the P3HT (010) peak from 1.66 to 1.68 Q, indicating that this intercalation-induced phase transition does not take place. Additionally, for our DDB-F_{72}-doped films, we observe a small shift in the P3HT (100) lamellar peak to higher Q (see inset), which is in the opposite direction of what is typically seen with F_4TCNQ doping.[9,15] This provides a clear indication that, unlike F_4TCNQ, DDB-F_{72} does not intercalate into the P3HT lamellar regions. The lack of intercalation of large molecular structures into the polymer crystallites is not surprising as their size does not allow them to fit between P3HT side chains. Furthermore, previous work has shown that addition of bulky groups on fullerenes can inhibit their intercalation into the lamellar regions of conjugated polymers,[46] and molecules of DDB-F_{72} have approximately twice the diameter of a typical fullerene. Overall, the observed peak shifts suggest that for DDB-F_{72}, the structural changes induced by doping are solely due to the delocalization of charges within a crystallite,[9,15] likely accompanied by counterions situated around the edge of each doped crystallite.

At high (1×10^{-3} M) DDB-F_{72} dopant solution concentration, we see a significant loss of crystallinity and a broadening of the P3HT (100) peak rather than a shift. Since GIWAXS only reports on crystalline regions in the doped films, the broadening we observe suggests that at this high doping concentration, most of the doped regions have become amorphous and the only remaining P3HT crystallites seen via GIWAXS are those that remain undoped. The large increase in disordered P3HT π-stacking intensity seen between 1.2 and 1.5 Q further supports the idea that these high-concentration-doped films are much more disordered than those doped using solutions with lower concentrations of DDB-F_{72}.

Interestingly, we also observe the appearance of new peaks at 0.6 and 1.0 Q (marked by asterisks in Figure 2b) when P3HT is doped with DDB-F_{72}. These new peaks are broadened to the same extent and show a very similar texture as the P3HT peaks. The new peaks do not at all resemble those seen for DDB-F_{72} crystallites (see the Supporting Information). Therefore, we hypothesize that these new peaks either result from a new polymorph of P3HT that preferentially forms in the presence of DDB-F_{72} or a P3HT polymorph that is stable only at very high doping levels.

To characterize the extent of charge carrier delocalization in DDB-F_{72}-doped films, we turn to spectroscopic measurements. Spano and co-workers have argued theoretically that the degree of delocalization of holes on P3HT is directly reflected in the shape and position of the polaron's IR absorption spectrum.[15,21,47–49] Their predictions for how the spectral shape changes when the polarons are localized by proximity to an anion, reproduced from ref. [15], are shown in **Figure 3**b, where the blue curve shows the spectrum of a fully delocalized P3HT polaron with no confinement by an anion. We have shown previously using F_4TCNQ-doped P3HT films with different crystallinities that the spectrum of polarons with different degrees of delocalization matches well with Spano and co-workers' theory, and indeed correlates strongly with the experimentally measured polaron mobility.[15]

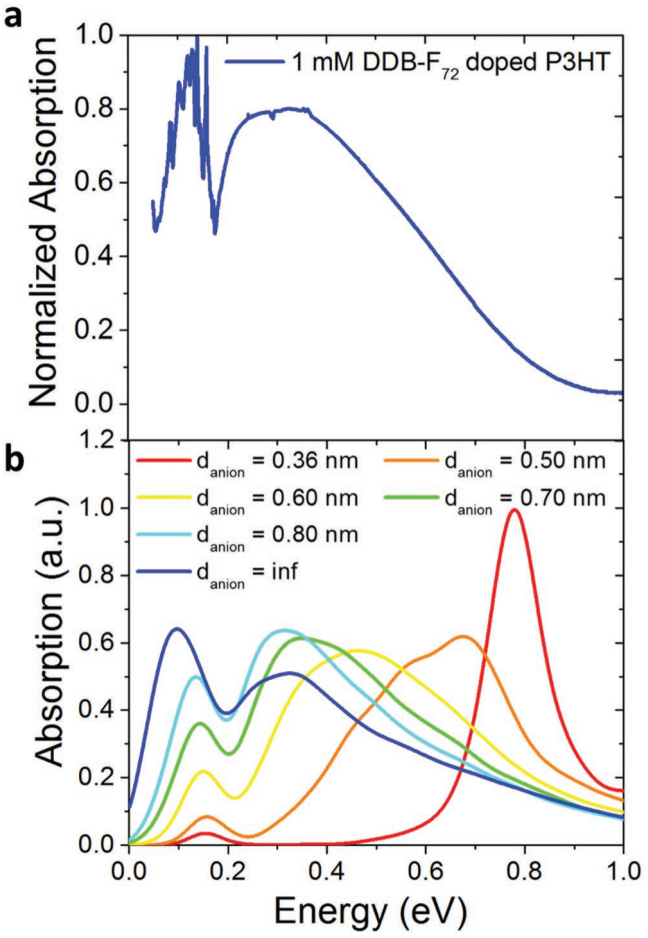

Figure 3. Delocalized polaron IR-spectrum. a) Experimental IR absorption spectrum of the polaron in a 1×10^{-3} M DDB-F_{72}-doped P3HT film. b) Simulated P3HT polaron absorption spectrum for different anion–polaron distances, taken from ref. [15]. The measured spectrum is in excellent agreement with the theoretical spectrum for an anion at infinite distance, indicating that the polarons in the chemically doped DDB-F_{72} sample are as delocalized as possible. Note: A distance-dependent permittivity for the pure polymer was used for the calculation. Although the use of a different permittivity would change the shape of the spectrum of the more Coulomb-localized polarons, the spectrum calculated for infinite anion distance is invariant with respect to the choice of permittivity.[15]

Figure 3a shows the measured IR spectrum of our DDB-F_{72}-doped P3HT films. The shape and position of the spectrum we measure is essentially identical to that predicted for a fully delocalized polaron that has no Coulombic interaction with an anion. Indeed, similar IR spectra have been measured in P3HT films doped by charge modulation with no anion present (i.e., doped by the presence of a large applied voltage).[11] A similar polaron spectrum also has been observed in recent work doping P3HT with large molybdenum dithiolene complexes, although the conductivities were much lower than we see here, likely due to low carrier densities, and carrier mobilities were not reported.[38] This indicates that the electron on the DDB-F_{72} anion is sufficiently isolated to have no effect on the polaron, despite the relatively low dielectric constant of P3HT. This is because the electron is localized entirely in the cluster interior, which by Gauss' law means that it effectively behaves as a point charge at the center of the cluster. The steric bulk associated with the substituted DDB cluster means that at no point can the polaron–anion distance be less than the radius of the cluster, which is ≈1 nm. We believe that it is the combination of electron localization to the dopant interior, shielded by the bulky substituents, with the fact that the dopants sit outside the P3HT crystallites that leads to this unusual but highly favorable situation where the polaron is entirely unaffected by the dopant counterion.

Table 1. Comparison of carrier density (n), mobility (μ), and conductivity (σ) measured by the AC Hall effect for P3HT films doped with DDB-F_{72} and F_4TCNQ at their respective solubility limits in DCM. Also shown is the number density of dopant molecules in the film estimated via mass measurements (N_{est}); see the Supporting Information for details. The F_4TCNQ data is taken from ref. [14].

Dopant	n [1 cm^{-3}]	μ [cm^2 V^{-1} s^{-1}]	σ [S cm^{-1}]	N_{est} [1 cm^{-3}]
1×10^{-3} M DDB-F_{72}	7.9×10^{20}	0.10	12.8	$6.9(6) \times 10^{20}$
3.6×10^{-3} M[a)] F_4TCNQ[14]	4.3×10^{20}	0.02	1.5	$4.8(9) \times 10^{21}$

[a)]3.6×10^{-3} M = 1 mg mL^{-1} F_4TCNQ.

To further characterize the extent of delocalization of the polarons in our DDB-F_{72}-doped P3HT films, we performed AC Hall effect measurements,[50–53] the results of which for identically prepared F_4TCNQ- and DDB-F_{72}-doped P3HT films[14] are summarized in **Table 1**. The concentrations chosen for both dopants were their solubility limits in DCM. We note that for low-mobility materials such as doped conjugated polymers, screening effects can cause Hall effect measurements to slightly overestimate the mobile carrier concentration and thus slightly underestimate the free carrier mobility,[53] as discussed in more detail in the Supporting Information.

In our P3HT sample doped with 1×10^{-3} M DDB-F_{72}, we measure a mobile carrier concentration that is roughly twice that of the F_4TCNQ-doped sample. We believe that this results from a higher ratio of integer charge transfer due to the greater energetic driving force for doping with DDB-F_{72}, summarized in Figure 1a, and an increase in free carrier (as opposed to trapped carrier) generation due to less Coulomb interaction with DDB-F_{72}. In fact, we have estimated the overall concentration of dopant clusters in the film by directly measuring the change in mass upon doping the films (see the Supporting Information for details). For F_4TCNQ, the dopant density is $4.8(9) \times 10^{21}$ cm^{-3} yielding a doping efficiency of ≈10% (slightly higher than the 5% value determined by Pingel and Neher[16,17] likely due to the fact that we are in a much higher doping regime and/or to the potential overestimation of the free carrier concentration via AC Hall measurements[53]). For DDB-F_{72}, the dopant concentration is $6.9(6) \pm 1.2 \times 10^{20}$ cm^{-3}, which agrees within error with the carrier concentration we measure via the AC Hall effect (which we also expect to be slightly overestimated[53]). This strongly suggests that essentially every DDB-F_{72} dopant molecule gives rise to a free polaron on P3HT, a full order of magnitude improvement over the ≈5–10% free carrier yield estimated for F_4TCNQ.

Perhaps more importantly, the carrier mobility of 0.1 cm^2 V^{-1} s^{-1} is five times higher for DDB-F_{72} than F_4TCNQ, a direct reflection of the higher degree of polaron delocalization with

DDB-F_{72}. Moreover, the polaron mobility in the DDB-F_{72}-doped P3HT films is comparable to mobilities seen only in charge-modulation-doped films with no anions present[11] or in highly crystalline doped 100% regioregular P3HT.[15] Finally, the large degree of polaron delocalization is also supported by the results of temperature-dependent conductivity experiments, which are discussed in the Supporting Information.

Overall, we have demonstrated that by using a functionalized dodecaborane dopant, we can achieve spatial separation of the conjugated polymer polaron and counterion leading to highly delocalized and mobile charge carriers even in poorly crystalline polymer material. The dodecaborate cluster anions cannot infiltrate into P3HT crystallites, resulting in a substantial loss in crystallinity upon doping. Thus, the counterions reside outside any remaining P3HT crystallites, and the unpaired electron on the DDB-F_{72} anion is further separated from the polarons on the polymer by being confined to the cluster core. The shielding provided by the cluster's physical and electronic structure relaxes the crystallinity constraints typically needed to achieve high conductivities and mobilities in doped conjugated polymer materials. Thus, with other dopants such as F_4TCNQ, crystallinity is important both for improving the delocalization of the polarons and for keeping the anion as far from the polymer backbone as possible. With our dodecaborane cluster dopant, on the other hand, we see that reducing the polaron localization by the anion is at least as important as delocalization due to crystallinity in determining polaron mobility and thus overall conductivity. We achieve conductivities of 12.8 S cm^{-1} and mobilities of 0.1 cm^2 V^{-1} s^{-1} with our DDB-F_{72}-doped P3HT, values that are an order of magnitude higher than those obtained with comparable doping by F_4TCNQ. Since the DDB-F_{72}-doped P3HT films significantly increase in thickness upon doping and the DDB clusters themselves do not conduct, this means that the idealized P3HT hole conductivities reach 32 S cm^{-1}. Thus, by carefully designing new molecular dopants, we can produce stable molecularly doped conjugated polymer films with polaron mobilities limited only by intrinsic materials properties, rather than being limited by electrostatic attraction to the proximal dopant anion.

Experimental Section

Details of the materials, synthesis, and characterization and experimental methods for device fabrication, electrical, structural, and spectroscopic measurements, as well as TD-DFT calculations can be found in the Supporting Information.

Supporting Information

Supporting Information is available from the Wiley Online Library or from the author.

Acknowledgements

This work was supported by the National Science Foundation under awards CHE-1608957 and CBET-1510353. The authors thank Alex I. Wixtrom and Miles Savage for assistance with synthesis of DDB-F_{72}. Use of the Stanford Synchrotron Radiation Lightsource, SLAC National Accelerator Laboratory was supported by the U.S. Department of Energy, Office of Science, Office of Basic Energy Sciences under Contract No. DE-AC02-76SF00515. J.-Y.L. thanks the CSC Fellowship. A.N.A. thanks the NSF CAREER Award CHE-1351968. TD-DFT calculations were performed using Extreme Science and Engineering Discovery Environment's (XSEDE) computing resources. A.M.S. thanks 3M Non-tenured Faculty Award, Alfred P. Sloan Foundation (Fellowship in Chemistry), and Research Corporation for Science Advancement (Cottrell Scholar).

Conflict of Interest

The authors declare no conflict of interest.

Keywords

Coulomb screening, dodecaboranes, molecular dopants, mobility, semiconducting polymers

Received: August 30, 2018
Revised: December 7, 2018
Published online:

[1] B. Lüssem, M. Riede, K. Leo, *Doping of Organic Semiconductors*, Vol. *210*, PSS (Physica Status Solidia), Dresden, Germany **2013**.
[2] Y. Zhang, H. Zhou, J. Seifter, L. Ying, A. Mikhailovsky, A. J. Heeger, G. C. Bazan, T. Q. Nguyen, *Adv. Mater.* **2013**, *25*, 7038.
[3] L. Ma, W. H. Lee, Y. D. Park, J. S. Kim, H. S. Lee, K. Cho, *Appl. Phys. Lett.* **2008**, *92*, 1.
[4] A. M. Glaudell, J. E. Cochran, S. N. Patel, M. L. Chabinyc, *Adv. Energy Mater.* **2015**, *5*, 4.
[5] S. N. Patel, A. M. Glaudell, K. A. Peterson, E. M. Thomas, K. A. O'Hara, E. Lim, M. L. Chabinyc, *Sci. Adv.* **2017**, *3*, 24.
[6] G. Zuo, O. Andersson, H. Abdalla, M. Kemerink, *Appl. Phys. Lett.* **2018**, *112*, 2.
[7] J. Hynynen, D. Kiefer, C. Müller, *RSC Adv.* **2018**, *8*, 1593.
[8] E. Lim, K. A. Peterson, G. M. Su, M. L. Chabinyc, *Chem. Mater.* **2018**, *30*, 998.
[9] A. Hamidi-Sakr, L. Biniek, J. L. Bantignies, D. Maurin, L. Herrmann, N. Leclerc, P. Lévêque, V. Vijayakumar, N. Zimmermann, M. Brinkmann, *Adv. Funct. Mater.* **2017**, *27*, 1.
[10] J. D. Yuen, A. S. Dhoot, E. B. Namdas, N. E. Coates, M. Heeney, I. McCulloch, D. Moses, A. J. Heeger, *J. Am. Chem. Soc.* **2007**, *129*, 14367.
[11] J. F. Chang, J. Clark, N. Zhao, H. Sirringhaus, D. W. Breiby, J. W. Andreasen, M. M. Nielsen, M. Giles, M. Heeney, I. McCulloch, *Phys. Rev. B: Condens. Matter Mater. Phys.* **2006**, *74*, 1.
[12] C. K. Chiang, S. C. Gau, C. R. Fincher, Y. W. Park, A. G. MacDiarmid, A. J. Heeger, *Appl. Phys. Lett.* **1978**, *33*, 18.
[13] V. V. Kislyuk, O. P. Dimitriev, A. A. Pud, J. Lautru, I. Ledoux-Rak, *J. Phy.: Conf. Ser.* **2011**, *286*, 1.
[14] D. T. Scholes, S. A. Hawks, P. Y. Yee, H. Wu, J. R. Lindemuth, S. H. Tolbert, B. J. Schwartz, *J. Phys. Chem. Lett.* **2015**, *6*, 4786.
[15] D. T. Scholes, P. Y. Yee, J. R. Lindemuth, H. Kang, J. Onorato, R. Ghosh, C. K. Luscombe, F. C. Spano, S. H. Tolbert, B. J. Schwartz, *Adv. Funct. Mater.* **2017**, *27*, 1.
[16] P. Pingel, D. Neher, *Phys. Rev. B* **2013**, *87*, 1.
[17] P. Pingel, M. Arvind, L. Kölln, R. Steyrleuthner, F. Kraffert, J. Behrends, S. Janietz, D. Neher, *Adv. Electron. Mater.* **2016**, *2*, 1600204.

[18] A. Mityashin, Y. Olivier, T. Van Regemorter, C. Rolin, S. Verlaak, N. G. Martinelli, D. Beljonne, J. Cornil, J. Genoe, P. Heremans, *Adv. Mater.* **2012**, *24*, 1535.
[19] I. E. Jacobs, E. W. Aasen, J. L. Oliveira, T. N. Fonseca, J. D. Roehling, J. Li, G. Zhang, M. P. Augustine, M. Mascal, A. J. Moulé, *J. Mater. Chem. C* **2016**, *4*, 3454.
[20] J. Hynynen, D. Kiefer, L. Yu, R. Kroon, R. Munir, A. Amassian, M. Kemerink, C. Müller, *Macromolecules* **2017**, *50*, 8140.
[21] A. R. Chew, R. Ghosh, Z. Shang, F. C. Spano, A. Salleo, *J. Phys. Chem. Lett.* **2017**, *8*, 4974.
[22] K. Kang, S. Watanabe, K. Broch, A. Sepe, A. Brown, I. Nasrallah, M. Nikolka, Z. Fei, M. Heeney, D. Matsumoto, K. Marumoto, H. Tanaka, S. I. Kuroda, H. Sirringhaus, *Nat. Mater.* **2016**, *15*, 896.
[23] W. Gao, A. Kahn, *Appl. Phys. Lett.* **2001**, *79*, 4040.
[24] R. B. King, *Chem. Rev.* **2001**, *101*, 1119.
[25] T. Peymann, C. B. Knobler, S. I. Khan, M. F. Hawthorne, *Angew. Chem., Int. Ed.* **2001**, *40*, 1664.
[26] T. Peymann, C. B. Knobler, M. F. Hawthorne, *Chem. Commun.* **1999**, *12*, 2039.
[27] N. Van, I. Tiritiris, R. F. Winter, B. Sarkar, P. Singh, C. Duboc, A. Muñoz-Castro, R. Arratia-Pérez, W. Kaim, T. Schleid, *Chem. - Eur. J.* **2010**, *16*, 11242.
[28] O. K. Farha, R. L. Julius, M. W. Lee, R. E. Huertas, C. B. Knobler, M. F. Hawthorne, *J. Am. Chem. Soc.* **2005**, *127*, 18243.
[29] J. C. Axtell, L. M. A. Saleh, E. A. Qian, A. I. Wixtrom, A. M. Spokoyny, *Inorg. Chem.* **2018**, *57*, 2333.
[30] D. Jung, L. M. A. Saleh, Z. J. Berkson, M. F. El-Kady, J. Y. Hwang, N. Mohamed, A. I. Wixtrom, E. Titarenko, Y. Shao, K. McCarthy, J. Guo, I. B. Martini, S. Kraemer, E. C. Wegener, P. Saint-Cricq, B. Ruehle, R. R. Langeslay, M. Delferro, J. L. Brosmer, C. H. Hendon, M. Gallagher-Jones, J. Rodriguez, K. W. Chapman, J. T. Miller, X. Duan, R. B. Kaner, J. I. Zink, B. F. Chmelka, A. M. Spokoyny, *Nat. Mater.* **2018**, *17*, 341.
[31] M. S. Messina, J. C. Axtell, Y. Wang, P. Chong, A. I. Wixtrom, K. O. Kirlikovali, B. M. Upton, B. M. Hunter, O. S. Shafaat, S. I. Khan, J. R. Winkler, H. B. Gray, A. N. Alexandrova, H. D. Maynard, A. M. Spokoyny, *J. Am. Chem. Soc.* **2016**, *138*, 6952.
[32] O. Khatib, B. Lee, J. Yuen, Z. Q. Li, M. Di Ventra, A. J. Heeger, V. Podzorov, D. N. Basov, *J. Appl. Phys.* **2010**, *107*, 12.
[33] C. Y. Kao, B. Lee, L. S. Wielunski, M. Heeney, I. McCulloch, E. Garfunkel, L. C. Feldman, V. Podzorov, *Adv. Funct. Mater.* **2009**, *19*, 1906.
[34] S. A. Hawks, J. C. Aguirre, L. T. Schelhas, R. J. Thompson, R. C. Huber, A. S. Ferreira, G. Zhang, A. A. Herzing, S. H. Tolbert, B. J. Schwartz, *J. Phys. Chem. C* **2014**, *118*, 17413.
[35] J. C. Aguirre, S. A. Hawks, A. S. Ferreira, P. Yee, S. Subramaniyan, S. A. Jenekhe, S. H. Tolbert, B. J. Schwartz, *Adv. Energy Mater.* **2015**, *5*, 1402020.
[36] T. J. Aubry, A. S. Ferreira, P. Y. Yee, J. C. Aguirre, S. A. Hawks, M. T. Fontana, B. J. Schwartz, S. H. Tolbert, *J. Phys. Chem. C* **2018**, *122*, 15078.
[37] P. Reiser, L. Müller, V. Sivanesan, R. Lovrincic, S. Barlow, S. R. Marder, A. Pucci, W. Jaegermann, E. Mankel, S. Beck, *J. Phys. Chem. C* **2018**, *122*, 14518.
[38] Z. Liang, Y. Zhang, M. Souri, X. Luo, A. M. Boehm, R. Li, Y. Zhang, T. Wang, D. Y. Kim, J. Mei, S. R. Marder, K. R. Graham, *J. Mater. Chem. A* **2018**, *6*, 16495.
[39] L. Müller, D. Nanova, T. Glaser, S. Beck, A. Pucci, A. K. Kast, R. R. Schröder, E. Mankel, P. Pingel, D. Neher, W. Kowalsky, R. Lovrincic, *Chem. Mater.* **2016**, *28*, 4432.
[40] M. Kivala, C. Boudon, J.-P. Gisselbrecht, B. Enko, P. Seiler, I. B. Müller, N. Langer, P. D. Jarowski, G. Gescheidt, F. Diederich, *Chem. - Eur. J.* **2009**, *15*, 4111.
[41] L. J. Van der Pauw, *Philips Tech. Rev.* **1958**, *20*, 220.
[42] V. A. Kolesov, C. Fuentes-Hernandez, W. F. Chou, N. Aizawa, F. A. Larrain, M. Wang, A. Perrotta, S. Choi, S. Graham, G. C. Bazan, T. Q. Nguyen, S. R. Marder, B. Kippelen, *Nat. Mater.* **2017**, *16*, 474.
[43] J. C. Goeltz, C. J. Hanson, C. P. Kubiak, *Inorg. Chem.* **2009**, *48*, 4763.
[44] J. C. Goeltz, E. E. Benson, C. P. Kubiak, *J. Phys. Chem. B* **2010**, *114*, 14729.
[45] T. M. Porter, G. C. Canzi, S. A. Chabolla, C. P. Kubiak, *J. Phys. Chem. A* **2016**, *120*, 6309.
[46] N. C. Miller, E. Cho, R. Gysel, C. Risko, V. Coropceanu, C. E. Miller, S. Sweetnam, A. Sellinger, M. Heeney, I. McCulloch, J.-L. Brédas, M. F. Toney, M. D. McGehee, *Adv. Energy Mater.* **2012**, *2*, 1208.
[47] C. M. Pochas, F. C. Spano, *J. Chem. Phys.* **2014**, *140*, 24.
[48] R. Ghosh, C. M. Pochas, F. C. Spano, *J. Phys. Chem. C* **2016**, *120*, 11394.
[49] R. Ghosh, A. R. Chew, J. Onorato, V. Pakhnyuk, C. K. Luscombe, A. Salleo, F. C. Spano, *J. Phys. Chem. C* **2018**, *122*, 18048.
[50] J. Lindemuth, *Proc. SPIE* **2012**, *8470*, 84700G.
[51] Y. Chen, H. T. Yi, V. Podzorov, *Phys. Rev. Appl.* **2016**, *5*, 1.
[52] F. Werner, *J. Appl. Phys.* **2017**, *122*, 13.
[53] H. T. Yi, Y. N. Gartstein, V. Podzorov, *Sci. Rep.* **2016**, *6*, 1.